



Magnesium silicate doped with environmentally friendly extractants used for rare earth elements adsorption

Andreea Gabor^a, Corneliu Mircea Davidescu^{a,*}, Adina Negrea^a, Mihaela Ciopec^a,
Cornelia Muntean^{a,*}, Petru Negrea^a, Catalin Ianasi^b, Monica Butnariu^c

^aPolitehnica University of Timisoara, Faculty of Industrial Chemistry and Environmental Engineering, 2 Piata Victoriei, RO 300006 Timisoara, Romania, Tel. +40 256 404147; emails: corneliu.davidescu@upt.ro, corneliu.davidescu@gmail.com (C.M. Davidescu), Tel. +40 256 404164; emails: cornelia.muntean@upt.ro, cornelia.muntean@yahoo.com (C. Muntean), emails: emeline_gabor@yahoo.com (A. Gabor), adina.negrea@upt.ro (A. Negrea), mihaela.ciopec@upt.ro (M. Ciopec), petru.negrea@upt.ro (P. Negrea)

^bInstitute of Chemistry Timisoara of Romanian Academy, Romanian Academy, 24 Blvd. Mihai Viteazul, RO 300223 Timisoara, Romania, email: cianasic@yahoo.com

^cBanat's University of Agricultural Sciences and Veterinary Medicine "King Michael I of Romania" from Timisoara, 119 Calea Aradului, RO 300645 Timisoara, Romania, email: monicabutnariu@yahoo.com

Received 15 May 2016; Accepted 13 August 2016

ABSTRACT

New adsorbent materials using different doping methods were obtained. Magnesium silicate was doped with environmentally friendly extractants like sodium β -glycerophosphate, tetraethylammonium bromide, and thiourea. The methods used were the dry method, the ultrasound unconventional method, and a new method, the pellicular vacuum solvent vaporization. The doped materials were characterized by Fourier transform infrared spectroscopy (FTIR), scanning electron microscopy (SEM), energy dispersive X-ray analysis (EDX), and determination of the specific surface area (BET). The usefulness of these materials and their performances were studied on the adsorption of rare earth elements Eu(III), Nd(III), and La(III). The best adsorption capacity of 16 mg/g was obtained for Eu(III) on magnesium silicate doped with thiourea. Nonlinear regression analysis of adsorption data was made employing Langmuir, Freundlich and Sips models.

Keywords: Rare earth elements; Magnesium silicate; Extractant; Adsorption; Adsorption isotherm

1. Introduction

Numerous studies highlight that rare earth elements (REEs) are being used in high technology applications [1]. This includes catalyst, glassmaking, lighting and metallurgy, battery alloys, ceramics, and permanent magnets [2]. REEs are found in earth's crust with many reserves in about 34 countries [1]. It is also known that REEs can be used as fertilizers in agriculture [3] and as reagents in magnetic resonance imaging (MRI), in the medical field [4].

REEs can be removed from wastewater through traditional methods such as precipitation with chemical reagents,

ion exchange [1], liquid-liquid extraction [3], biosorption [5], and adsorption [6]. Some methods such as alkaline precipitation have disadvantages like low efficiency, high consumption of chemical reagents, and high costs. Adsorption is known as an advanced method for treatment of wastewater with REEs, featuring a number of advantages, namely: high efficiency, high adsorption capacity, the possibility of regeneration and use of adsorbents in multiple adsorption-desorption cycles, and selectivity for rare metals [6].

It is known that magnesium silicate possesses adsorption properties. Various studies revealed it in adsorption of dyes [7], phenols [8], and metals [9].

In order to improve the adsorption properties of inorganic supports, doping with various functional groups

* Corresponding author.

containing nitrogen, phosphorus and sulfur is employed. In the literature are described various doping methods like co-precipitation [10], dry method [11], and unconventional methods such as the use of ultrasounds [12].

In the present work, magnesium silicate has been doped with groups containing nitrogen in the form of tetraethylammonium bromide, phosphorus in the form of sodium β -glycerophosphate, and groups with sulfur and nitrogen in the form of thiourea. These extractants are considered green, being environmentally friendly [13]. From the literature, it is known that quaternary ammonium salts are used in two-phase system for the extraction of metals [14–16]. Compounds with phosphorus in the form of sodium β -glycerophosphate have applications especially in the medical field [17–22], and compounds with sulfur as thiourea are mainly used in metal extraction such as gold, copper, and rhodium [23–25].

The goals of this study were the removal of REEs Eu(III), La(III), and Nd(III) from aqueous solutions by adsorption on magnesium silicate doped with extractants containing N, P and S, and to compare the performance of the obtained new adsorbent materials. For this purpose, the influence of the doping method as well as the nature of the dissolving solvent and the nature of the extractant on the adsorption capacity of the obtained materials were studied. The novelty of this paper consists in the use of the above-mentioned extractants for doping magnesium silicate, not mentioned before in literature for this use. The methods used for doping were the well-known dry method, an unconventional method using ultrasounds, and a novel method, the pellicular vacuum vaporization of solvent.

2. Materials and methods

2.1. Materials

Magnesium silicate purchased as Florisil (0.150–0.250 mm) (Merck, Darmstadt, Germany) was used as inorganic support.

The following extractants were used (Table 1): tetraethylammonium bromide (99%, Merck, Darmstadt, Germany),

sodium β -glycerophosphate (99%, Merck, Darmstadt, Germany), thiourea (98%, Merck, Darmstadt, Germany). To dissolve the extractant, several solvents were used: absolute ethanol (99.2%, SC PAM Corporation SRL, Romania), acetone (100%, VWR Prolabo Chemicals, France), toluene (VWR Prolabo Chemicals, France), n-hexane (Merck, Darmstadt, Germany). REEs solutions of 1,000 mg/L concentration were used: lanthanum standard for AAS (Analytical Fluka, Sigma-Aldrich. co. LLC St. Louis, MO, USA); europium standard for AAS (VWR Prolabo Chemicals, Belgium); neodymium standard for AAS (VWR Prolabo Chemicals, Belgium). To prepare solutions of different concentrations, distilled water was used.

The support material was doped using different methods. For doping using ultrasounds, an ultrasonic bath SONOREX SUPER 10 P Bandelin was employed. The doping by pellicular vacuum solvent vaporization was performed using a Heidolph rotary evaporator. The drying of the samples was carried out in an NITECH oven.

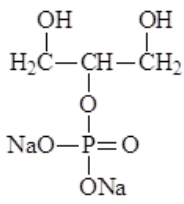
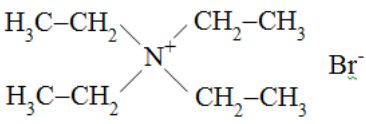
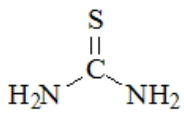
REEs adsorption on the doped materials was performed using a Julabo SW 23 shaker at 200 rot/min. REEs were analyzed by inductively coupled plasma-mass spectroscopy using an ICP-MS Bruker aurora M90 instrument.

2.2. Preparation of the doped materials

The doping of magnesium silicate was accomplished through the dry classical method, the unconventional method using ultrasounds, and a new method, the pellicular vacuum solvent vaporization. The same amounts of reagents were used in all methods. Amounts of 0.05–0.2 g extractant were dissolved in 25 mL solvent and mixed with 5 g magnesium silicate.

Doping the material by the dry method [11,26–28] consists in keeping in contact the extractant dissolved in the solvent with the solid support for 24 h at ambient temperature (298 K). The suspension obtained was kept 24 h in an oven at 323 K, to evaporate the solvent and to dry the doped material.

Table 1
Materials used for the preparation of the doped sorbents

Support	Extractant	Abbreviation	Chemical structure
Magnesium silicate	Sodium glycerophosphate	β -Na- β -Gly-P	
	Tetraethylammonium bromide	TEABr	
	Thiourea	Thi	

For the method using ultrasounds, contact between support and dissolved extractant was 10 min in an ultrasonic bath with 35 Hz frequency at 298 K. The suspensions were then treated as for the dry method.

Doping the material by pellicular vacuum solvent vaporization was carried out as follows: extractant dissolved in solvent was mixed with the solid support for 10 min in a rotary evaporator at 323 K and atmospheric pressure, and then the solvent was evaporated at 323 K at a pressure of 2 Pa.

2.3. Characterization of the doped material

The doped materials were characterized by Fourier transform infrared spectroscopy (FTIR) in KBr using a Shimadzu Prestige-21 FTIR spectrophotometer in the range 4,000–400 cm^{-1} , by scanning electron microscopy (SEM) and energy dispersive X-ray spectroscopy (EDX) using an FEI Quanta FEG 250 instrument, and by specific surface area measurements (BET) using a Quantachrome NOVA 1200E instrument. In the present work, we present only the results for the materials obtained by pellicular solvent vaporization, using ethyl alcohol as solvent and a 0.2:5 g extractant: support ratio.

2.4. REEs batch adsorption studies

The influence of several parameters on the adsorption of REEs was studied in batch experiments: the nature of the solvent used to dissolve the extractant (ethyl alcohol, acetone, n-hexane, toluene); the extractant: solid support ratio

(0.05, 0.1, and 0.2 g extractant: 5 g magnesium silicate), the nature of the extractant (Na- β -Gly-P, TEABr, and Thi), the method used to dope the support, and the initial concentration of the REEs (10, 50, 100, 150, and 200 mg/L).

For this purpose, samples of 0.1 g doped materials were weighed and were mixed with 25 mL REEs solution (Eu(III), Nd(III), La(III)). The contact time was 1 h, at 298 K, after which the samples were filtered and the residual concentration of REEs was determined by inductively coupled plasma-mass spectroscopy.

3. Results and discussion

3.1. Characterization of the doped materials

3.1.1. SEM and EDX analysis

To prove the presence of the functional groups after doping magnesium silicate with the extractants (Na- β -Gly-P, TEABr, and Thi), X-ray energy dispersive spectroscopy was performed, as shown in Fig. 1.

The EDX spectra of the obtained doped materials reveal the presence of specific peaks for each extractant used. Besides peaks of magnesium silicate (O, Mg, Si), in Fig. 1(a) the N and Br peaks characteristic for the extractant TEABr are present. The same situation is seen in Figs. 1(b) and (c) were the peaks of Na and P appears, characteristic for the extractant Na- β -Gly-P and respectively, the peaks of N and S, characteristic for the extractant Thi.

Fig. 2 presents the surface morphology of magnesium silicate after doping. In contrast to the image of the support [26],

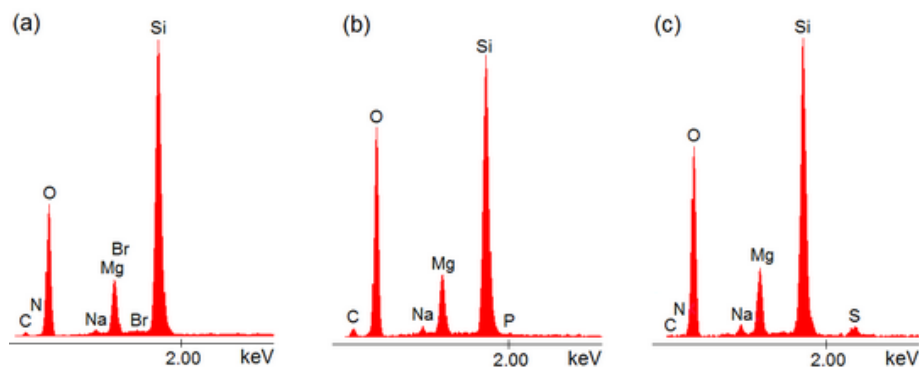


Fig. 1. EDX spectra of the materials obtained by doping magnesium silicate with different extractants: (a) TEABr; (b) Na- β -Gly-P; (c) Thi.

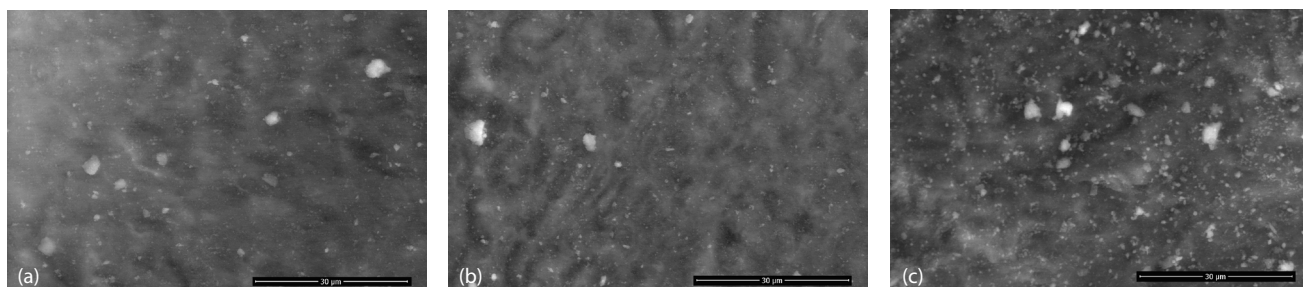


Fig. 2. Surface morphology of the materials obtained by doping magnesium silicate with different extractants: (a) TEABr; (b) Na- β -Gly-P; (c) Thi.

SEM images recorded after functionalization show white spots that confirm the presence of the extractants clusters on the surface of the support. Compared to the other extractants, Thi appears to be better dispersed on the support surface.

3.1.2. Fourier transform infrared spectroscopy

The FT-IR spectrum of commercial magnesium silicate (Figs. 3(a), 4(a), 5(a)) shows a broad band at $\sim 3,400\text{ cm}^{-1}$ assigned to O-H bond stretching vibrations. The large and intense $1,070\text{ cm}^{-1}$ band with a weak shoulder at $1,230\text{ cm}^{-1}$ and the band at 673 cm^{-1} are characteristic for stretching vibrations of Si-O bonds. The band from 800 cm^{-1} is assigned to bending vibrations of the Si-O-Si bonds. The vibration around $\sim 1,640\text{ cm}^{-1}$ represents d(O-H) vibrations in H_2O [29].

The FTIR spectrum of tetraethylammonium bromide (Fig. 3(b)) has two weak bands at $3,420$ and at $1,634\text{ cm}^{-1}$ assigned to O-H bond stretching and bending vibrations in H_2O (moisture), and a strong band at $2,984\text{ cm}^{-1}$ corresponding to the stretching vibration of the aliphatic C-H bond. The bands at $1,490, 1,443, 1,404, 1,373$ (shoulder), and $1,336$ (shoulder) cm^{-1} are characteristic for bending of CH_2 and CH_3 aliphatic groups. The bands at $1,176, 1,055,$ and $1,005\text{ cm}^{-1}$ may be assigned to the stretching of C-N bond in amines, and the bands at 899 and 793 cm^{-1} to the rock of CH_3 and CH_2 groups.

The FTIR spectrum profile of $\text{MgO}_3\text{Si} + \text{C}_8\text{H}_{20}\text{N}^+\text{Br}^-$ (Fig. 3(c)) shows that the bands of the components overlap. Some of the stronger characteristic bands of TEABr are still visible as weak bands at $2,997$ and $1,487\text{ cm}^{-1}$. The other extractant bands are overlapped by the support bands.

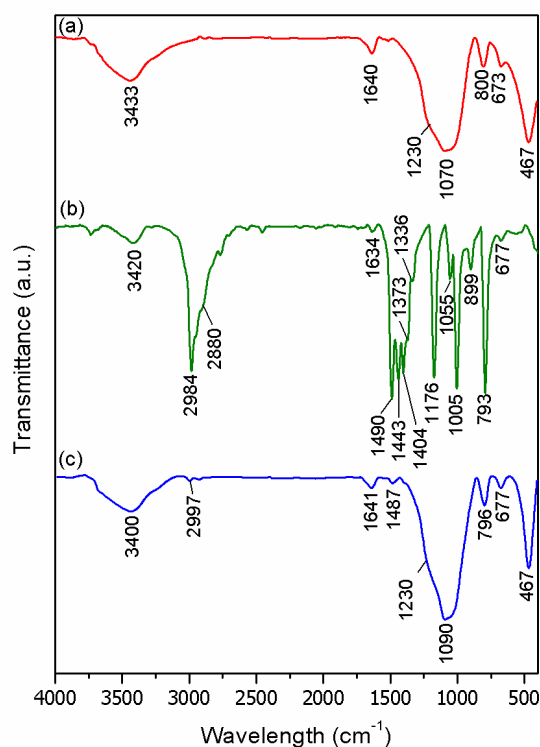


Fig. 3. FTIR spectra of the (a) solid support magnesium silicate, (b) TEABr extractant, and (c) doped material.

Thiourea shows wide bands in the IR spectrum (Fig. 4(b)) due to the C=S and C-N bonds, and NH_2 groups. The bands in the range $3,400\text{--}3,100\text{ cm}^{-1}$ correspond to antisymmetric and symmetric N-H stretching vibrations. The band at $1,616\text{ cm}^{-1}$ corresponds to $\delta(\text{NH}_2)$ vibration. The band at $1,471\text{ cm}^{-1}$ is assigned to asymmetric stretching of C-N bond. The bands of thiourea at $1,412$ and 731 cm^{-1} correspond to the antisymmetric and symmetric C-S stretching vibrations. The band at $1,082\text{ cm}^{-1}$ is associated to $\nu_s(\text{C-N})$. Other frequencies may be assigned as: 630 cm^{-1} $t(\text{NH}_2)$, 496 cm^{-1} $\delta_s(\text{S-C-N})$, and 453 cm^{-1} $\delta_s(\text{N-C-N})$ [30].

The spectrum of magnesium silicate doped with thiourea (Fig. 4(c)) shows the bands characteristic to the support, which overlap in most cases the bands of the extractant. Some of the most intense bands of thiourea are still visible, but they are very weak: $3,198, 1,406,$ and 735 cm^{-1} .

The FTIR spectrum of sodium β -glycerophosphate (Fig. 5(b)) shows characteristic vibrations of glycerine: O-H stretching at $3,200\text{--}3,400\text{ cm}^{-1}$, C-H stretching at $2,950$ and $2,874\text{ cm}^{-1}$, C-O stretching at $1,130\text{ cm}^{-1}$, CH_2 bend at $1,477\text{ cm}^{-1}$, O-H in-plane bending at $1,350\text{ cm}^{-1}$, and O-H out-of-plane bending at 770 cm^{-1} . Other bands may be assigned to: $1,680\text{ cm}^{-1}$ (O-H) bending in H_2O , $1,080\text{ cm}^{-1}$ P=O bond, 974 cm^{-1} P-O-R group [31,32]. The band at 528 cm^{-1} may be assigned to phosphate ν^4 stretching and the bands in the region $1,200\text{--}800\text{ cm}^{-1}$ to ν^4 stretching [22].

The IR spectrum of the mixture $\text{MgO}_3\text{Si} +$ sodium β -glycerophosphate (Fig. 5(c)) illustrates a visible overlapping of the absorption bands of the two components. The broad band around $3,300\text{ cm}^{-1}$ for O-H bond stretching and the

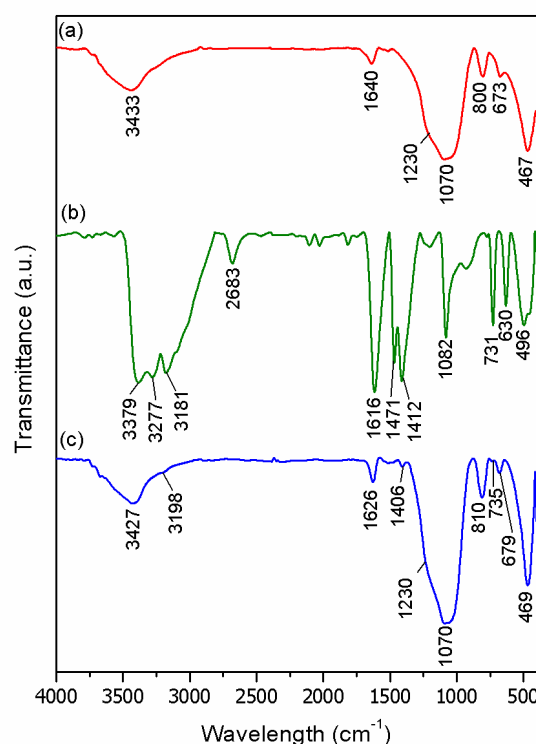


Fig. 4. FTIR spectra of the (a) solid support magnesium silicate, (b) Thi extractant, and (c) doped material.

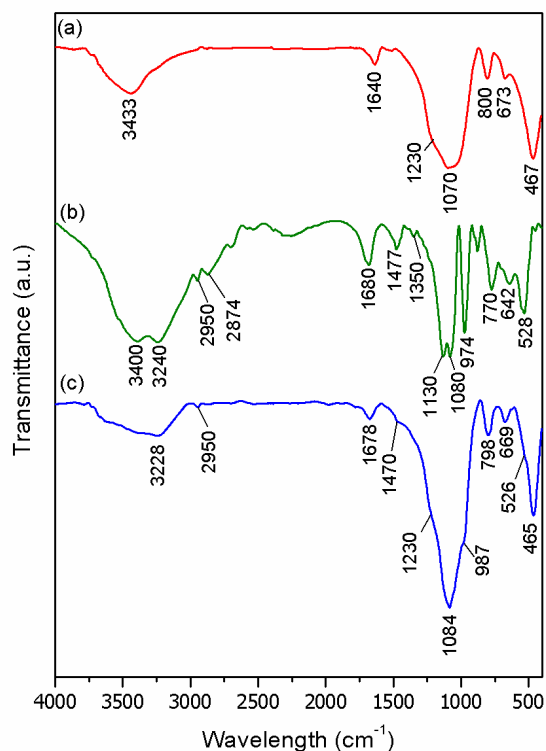


Fig. 5. FTIR spectra of the (a) solid support magnesium silicate, (b) Na-β-Gly-P extractant, and (c) doped material.

one at 1,678 cm^{-1} for O-H bending in H_2O are also present in the both spectra of the single components. In the range 1,550–400 cm^{-1} the bands are overlapped. Some of the bands of sodium β-glycerophosphate are still visible, but they are very weak or are shoulders of broader, more intense bands: 2,950, 1,470, 987, and 526 cm^{-1} .

3.1.3. BET measurements

Using BET measurements, one can obtain data that give information about pore size distribution, surface area and total pore volume. Before measurements, all samples were degassed in vacuum for 5 h at room temperature. The presence of the hysteresis loop for support and the doped materials indicates a type IV isotherm (Fig. 6). According to IUPAC, this hysteresis is of type H3, which indicates slit shape pores or plate like particles [33]. Other information from hysteresis is that in H3 case, the sample does not have a limit of adsorption near 1 P/P_0 .

The results obtained for the doped samples are close (Table 2) and the values for all parameters are smaller than those of the support MgSiO_3 : surface area 230.15 m^2/g , average pore diameter 3.441 nm, total pore volume 0.4374 cm^3/g [26]. The surface area of the support determined with BET (Brunauer-Emmett-Teller) method decreased after doping from ~230 to ~190 m^2/g . The smallest specific surface area was obtained for the material doped with Thi, which seems better dispersed on the support surface (Fig. 2). The total pore volume also decreased from ~0.44 to ~0.39 cm^3/g .

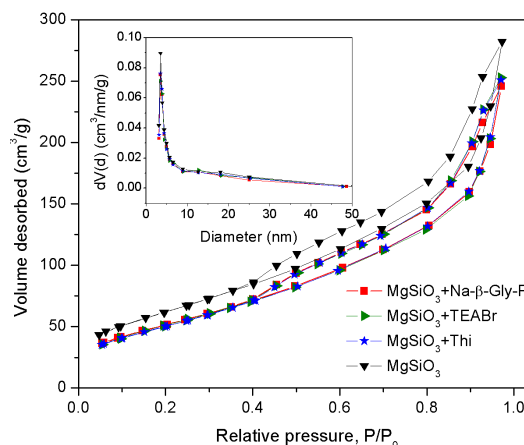


Fig. 6. Nitrogen adsorption-desorption isotherms and pore size distribution of the support and the doped materials.

Table 2

The surface area, pore diameter and total pores volume of the doped materials

Doped material	Surface area, m^2/g	Average pore diameter, nm	Total pore volume, cm^3/g
$\text{MgSiO}_3 + \text{Na-}\beta\text{-Gly-P}$	193.52	3.439	0.3813
$\text{MgSiO}_3 + \text{TEABr}$	193.72	3.436	0.3921
$\text{MgSiO}_3 + \text{Thi}$	190.03	3.425	0.3891

The shape of the isotherms did not change after doping, which suggests that the structure was maintained. This is also confirmed by the pore size distribution. Inset in Fig. 6 presents the pore size distribution calculated using the BJH (Barrett-Joyner-Halenda) method. It can be observed that for all samples the distribution is narrow, which leads us to suppose that the porosity is ordered and did not change after doping. The average pore size of all samples was around 3.4 nm.

The decrease of the specific surface area and the total pores volume, with maintaining of structure and pore size distribution, suggests that the extractants were attached to the surface of the support and entered into the largest pores, the smallest ones being only partially blocked.

3.2. REEs adsorption on the doped materials

3.2.1. Influence of extractant nature, solvent nature, extractant: support ratio, and doping method on the adsorption performance of the obtained materials

Data regarding the maximum adsorption capacity of the doped materials toward REEs depending on the extractant nature and solvent, as well as the extractant (g): support (g) (E:S) ratio for the doping methods used are listed in Tables 3–5.

The equilibrium adsorption capacity q_e (mg/g) was calculated using Eq. (1):

$$q_e = \frac{(C_0 - C_e)V}{m} \quad (1)$$

Table 3
Maximum adsorption capacities reached after doping by the dry method

Extractant	Solvents	Maximum adsorption capacity, q_m (mg/g)											
		Ethyl alcohol			Acetone			n-hexane			Toluene		
		E:S ratio	0.05:5	0.1:5	0.2:5	0.05:5	0.1:5	0.2:5	0.05:5	0.1:5	0.2:5	0.05:5	0.1:5
		Metal ion											
Na- β -Gly-P	Eu(III)	10.96	11.03	11.05	10.25	10.23	10.33	10.18	10.21	10.21	9.97	10.12	10.08
	Nd(III)	10.42	10.40	10.45	10.40	10.41	10.41	10.38	10.40	10.39	10.36	10.39	10.40
	La(III)	11.39	11.43	11.49	10.50	10.46	10.63	10.31	10.32	10.30	9.93	9.59	9.85
TEABr	Eu(III)	10.19	10.19	10.21	10.11	10.13	10.14	10.07	10.09	10.10	9.97	10.00	10.02
	Nd(III)	10.31	10.34	10.36	10.26	10.29	10.32	10.20	10.22	10.24	10.15	10.17	10.19
	La(III)	12.22	12.46	12.41	11.13	11.14	11.19	9.91	10.16	10.25	8.97	9.00	9.01
Thi	Eu(III)	10.21	10.23	10.25	10.18	10.20	10.22	10.07	10.09	10.11	9.95	9.97	9.99
	Nd(III)	10.45	10.47	10.50	10.41	10.43	10.45	10.33	10.36	10.39	10.25	10.27	10.30
	La(III)	10.46	10.48	10.47	10.20	10.21	10.23	10.21	10.20	10.25	9.99	9.99	9.74

Table 4
Maximum adsorption capacities reached after doping using ultrasounds

Extractant	Solvents	Maximum adsorption capacity, q_m (mg/g)											
		Ethyl alcohol			Acetone			n-hexane			Toluene		
		E:S ratio	0.05:5	0.1:5	0.2:5	0.05:5	0.1:5	0.2:5	0.05:5	0.1:5	0.2:5	0.05:5	0.1:5
		Metal ion											
Na- β -Gly-P	Eu(III)	2.85	2.87	2.91	2.78	2.79	2.81	2.73	2.74	2.76	2.63	2.65	2.67
	Nd(III)	5.18	5.19	5.21	5.12	5.14	5.16	5.06	5.09	5.11	4.95	4.99	5.03
	La(III)	4.46	4.49	4.51	4.39	4.40	4.41	4.32	4.34	4.35	4.23	4.25	4.27
TEABr	Eu(III)	5.21	5.23	5.25	4.96	4.98	5.01	4.82	4.84	4.86	4.74	4.75	4.76
	Nd(III)	6.79	6.81	6.83	6.72	6.74	6.76	6.59	6.62	6.64	6.49	6.51	6.53
	La(III)	9.64	9.68	9.70	9.57	9.58	9.60	9.49	9.51	9.53	9.35	9.37	9.39
Thi	Eu(III)	4.18	4.22	4.24	4.13	4.14	4.15	4.07	4.05	4.07	4.00	4.01	4.02
	Nd(III)	5.46	5.48	5.50	5.42	5.44	5.47	5.35	5.37	5.39	5.28	5.30	5.32
	La(III)	7.31	7.34	7.35	7.23	7.25	7.28	7.14	7.16	7.18	7.10	7.11	7.13

Table 5
Maximum adsorption capacities reached after doping by pellicular vacuum solvent vaporization

Extractant	Solvents	Maximum adsorption capacity, q_m (mg/g)											
		Ethyl alcohol			Acetone			n-hexane			Toluene		
		E:S ratio	0.05:5	0.1:5	0.2:5	0.05:5	0.1:5	0.2:5	0.05:5	0.1:5	0.2:5	0.05:5	0.1:5
		Metal ion											
Na- β -Gly-P	Eu(III)	13.53	13.56	13.58	13.49	13.50	13.51	13.32	13.36	13.36	13.33	13.33	13.34
	Nd(III)	11.41	11.46	11.50	11.28	11.30	11.32	11.19	11.21	11.23	11.10	11.09	11.11
	La(III)	10.64	10.68	10.69	10.59	10.62	10.64	10.57	10.58	10.60	10.50	10.52	10.53
TEABr	Eu(III)	15.58	15.60	15.62	15.48	15.50	15.52	15.37	15.38	15.40	15.24	15.26	15.28
	Nd(III)	13.12	13.14	13.16	13.09	13.12	13.15	13.05	13.05	13.08	13.00	13.02	13.04
	La(III)	10.64	10.68	10.69	10.60	10.61	10.63	10.49	10.50	10.53	10.41	10.44	10.45
Thi	Eu(III)	16.14	16.16	16.18	16.08	16.10	16.12	16.00	16.03	16.06	15.89	15.91	15.93
	Nd(III)	14.45	14.48	14.50	14.38	14.41	14.43	14.34	14.36	14.39	14.27	14.25	14.29
	La(III)	11.45	11.51	11.53	11.32	11.34	11.37	11.25	11.27	11.30	11.20	11.22	11.24

where C_0 and C_e (mg/L) are the initial concentration of REEs solution, and the concentration at equilibrium, V (L) is the volume of the solution, and m (g) is the amount of adsorbent material.

From the data, we concluded that regardless of the nature of the extractant and doping method, the largest adsorption capacity was reached when ethyl alcohol was used as a solvent for the extractant. In most cases, the increase of the extractant: support ratio from 0.05:5 to 0.2:5 led to an insignificant increase of adsorption capacity.

In the case of doping by the dry method, the adsorption capacity was between 10 and 12 mg/g. When using ultrasounds for doping, the adsorption capacity varied between 2 and 7 mg/g. When using the pellicular vacuum solvent vaporization for doping, the adsorption capacity was between 11 and 16 mg/g, this being the most efficient doping method.

However, we should mention that for lanthanum, the best results were obtained by doping with TEABr by the dry method (12.5 mg/g, Table 3). Adsorption capacities obtained for lanthanum in this study, using dry method and pellicular vacuum solvent vaporization, for all extractants dissolved in ethyl alcohol, were higher than those obtained previously (9.13 mg/g) using as extractant tetrabutylammonium dihydrogen phosphate dissolved in ethyl alcohol and the dry method [26].

3.2.2. Adsorption isotherms

An adsorption isotherm describes the amount of component adsorbed on the adsorbent surface vs. the adsorbate amount in the fluid phase at equilibrium. The equilibrium adsorption capacity q_e (mg/g) was calculated using Eq. (1). REEs adsorption isotherms of the materials doped using the pellicular vacuum solvent vaporization and the extractant dissolved in ethyl alcohol (extractant: support ratio 0.1:5 g) are shown in Fig. 7.

It can be observed that with increasing initial concentration of the metal solution, the adsorption capacity increases reaching the maximum adsorption capacity q_m for equilibrium concentrations above 60 mg/L. Among the studied metals, Eu(III) has been best adsorbed by the doped materials, yielding an adsorption capacity of 13.56 mg/g for the magnesium silicate doped with Na- β -Gly-P, 15.60 mg/g in the case of doping with TEABr and 16.16 mg/g in the case of doping with Thi. The lowest values were obtained for La(III) (10.68 mg/g) when using Na- β -Gly-P and TEABr as extractants and a higher value was obtained when using the extractant Thi (11.51 mg/g). Best adsorption capacities of all REEs studied metals were obtained in the case of doping the solid support, magnesium silicate, with thiourea.

3.2.3. Modeling of adsorption isotherms

In this paper, the experimental data were analyzed by Langmuir, Freundlich, and Sips (Langmuir-Freundlich) adsorption isotherm models.

The Langmuir model is the most commonly used and is based on the assumption that the adsorption takes place only until a monomolecular layer of adsorbate forms, all positions are energy equivalent and the surface is uniform, while the

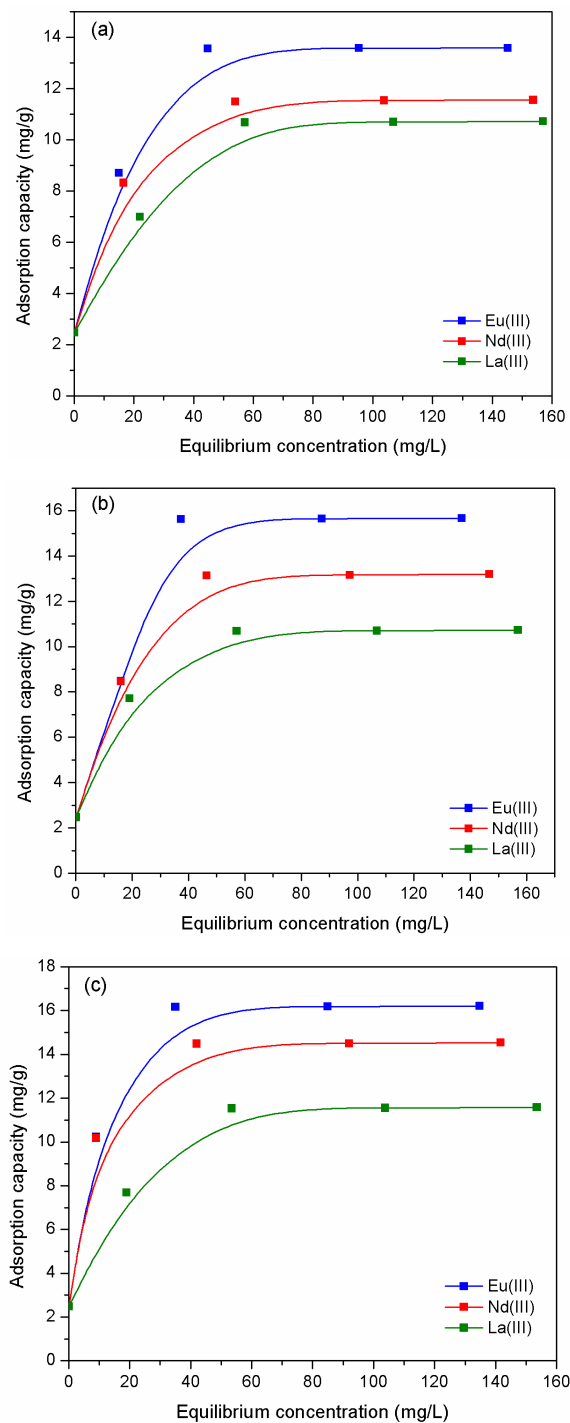


Fig. 7. Adsorption isotherms of REEs on magnesium silicate doped by pellicular vacuum solvent vaporization (a) Na- β -Gly-P; (b) TEABr; (c) Thi.

ability of a molecule to adsorb at a given position is independent of the occupying adjacent positions. Langmuir isotherm nonlinear expression is given by Eq. (2) [34]:

$$q_e = \frac{q_L K_L C_e}{1 + K_L C_e} \quad (2)$$

where q_e is the equilibrium adsorption capacity (mg/g), C_e is the equilibrium concentration of REEs in solution (mg/L), K_L is Langmuir constant and q_L is Langmuir maximum adsorption capacity (mg/g).

Another often-used isotherm is Freundlich isotherm, which describes the adsorbent surface as heterogeneous, and assumes that the distribution of adsorption heat is uneven and the process occurs as multilayer adsorption due to the unlimited reaction sites available. Freundlich isotherm nonlinear expression is given by Eq. (3) [35]:

$$q_e = K_F C_e^{1/n_F} \quad (3)$$

where K_F and n_F are the characteristic constants that can be related to the relative adsorption capacity of the adsorbent and the intensity of adsorption.

Sips isotherm is derived from Langmuir and Freundlich isotherm models. At low concentrations of adsorbate, it reduces to Freundlich isotherm, and at high concentrations, it predicts a monomolecular adsorption characteristic to the Langmuir isotherm. Sips isotherm nonlinear expression is given by Eq. (4) [36]:

$$q_e = \frac{q_s K_s C_e^{1/n_s}}{1 + K_s C_e^{1/n_s}} \quad (4)$$

where q_s is the maximum absorption capacity (mg/g), K_s is a constant related to the adsorption capacity of the adsorbent and n_s is the heterogeneity factor.

Nonlinear regression analysis was applied to determine the parameters of the Langmuir, Freundlich and Sips isotherms and the regression coefficients R^2 found in Tables 6–8 (the highest values of the regression coefficients are in bold). The parameters were used to calculate the Langmuir, Freundlich and Sips plots shown in Figs. 8–10 for each metal ion sorbed on the different adsorbent materials obtained.

The parameter values $1/n_F < 1$ and $1/n_s < 1$ indicate a high affinity of the adsorbents for REEs, a favorable adsorption and a convex isotherm for all REEs on all obtained materials, occupying first the highest energy positions then followed by those with less energy [37]. The values of the heterogeneity factors $1/n_F$ and $1/n_s$ are between 0.17 and 0.43. Their large deviation from 1 indicates that the surface of the obtained adsorbent material is highly heterogeneous. This is also seen in SEM images of the doped materials (Fig. 2), which show clusters of extractants on the surface of the support.

Data in Tables 6–8 show that for Nd(III) and La(III) adsorption, regardless of the extractant used for doping, and for Eu(III) adsorption onto magnesium silicate doped with Na-β-Gly-P, Langmuir isotherm has the lowest correlation coefficient R^2 , suggesting that this model gives the lowest fit of the adsorption data. Freundlich and Sips models have higher and close values for the correlation coefficient R^2 . This suggests that these isotherm models fit better the experimental data. In most cases, when the heterogeneity factor $1/n_s$ is higher, the Sips model gives a better fit than the Freundlich model. For Eu(III) adsorption onto magnesium silicate doped with TEABr and Thi, Langmuir model has the highest R^2 value and therefore better fits the experimental data. For

Table 6
Isotherm parameters for Eu(III) adsorption onto the doped materials

	Parameter	Na-β-Gly-P	TEABr	Thi
Experimental values				
	$q_{m,exp}$ (mg/g)	13.56	15.60	16.16
Isotherm model				
Langmuir	q_L (mg/g)	14.99	17.91	17.44
	K_L (L/mg)	0.109	0.0809	0.178
	R^2	0.8973	0.8936	0.9322
Freundlich	K_F (mg/g)	5.307	5.606	6.907
	$1/n_F$	0.205	0.224	0.192
	R^2	0.9156	0.8878	0.9073
Sips	q_s (mg/g)	20.93	29.90	21.64
	K_s	0.312	0.207	0.430
	$1/n_s$	0.385	0.363	0.434
	R^2	0.9135	0.8508	0.9308

Table 7
Isotherm parameters for Nd(III) adsorption onto the doped materials

	Parameter	Na-β-Gly-P	TEABr	Thi
Experimental values				
	$q_{m,exp}$ (mg/g)	11.46	13.14	14.48
Isotherm model				
Langmuir	q_L (mg/g)	12.32	14.59	15.26
	K_L (L/mg)	0.143	0.103	0.242
	R^2	0.8658	0.8798	0.9273
Freundlich	K_F (mg/g)	5.101	5.114	6.598
	$1/n_F$	0.176	0.206	0.176
	R^2	0.9476	0.9526	0.9219
Sips	q_s (mg/g)	17.46	24.79	18.31
	K_s	0.420	0.267	0.565
	$1/n_s$	0.326	0.312	0.423
	R^2	0.9577	0.9504	0.9677

Table 8
Isotherm parameters for La(III) adsorption onto the doped materials

	Parameter	Na-β-Gly-P	TEABr	Thi
Experimental values				
	$q_{m,exp}$ (mg/g)	10.64	10.64	11.51
Isotherm model				
Langmuir	q_L (mg/g)	12.11	11.56	12.83
	K_L (L/mg)	0.0737	0.122	0.0916
	R^2	0.8218	0.8454	0.8506
Freundlich	K_F (mg/g)	4.263	4.503	4.851
	$1/n_F$	0.194	0.186	0.185
	R^2	0.9289	0.9451	0.9364
Sips	q_s (mg/g)	33.38	16.59	27.46
	K_s	0.145	0.367	0.214
	$1/n_s$	0.248	0.340	0.259
	R^2	0.8979	0.9519	0.9139

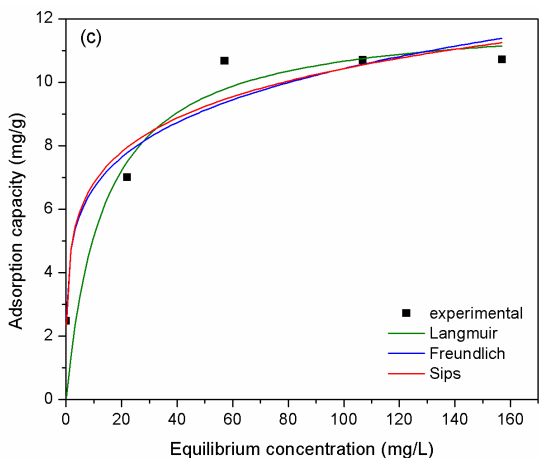
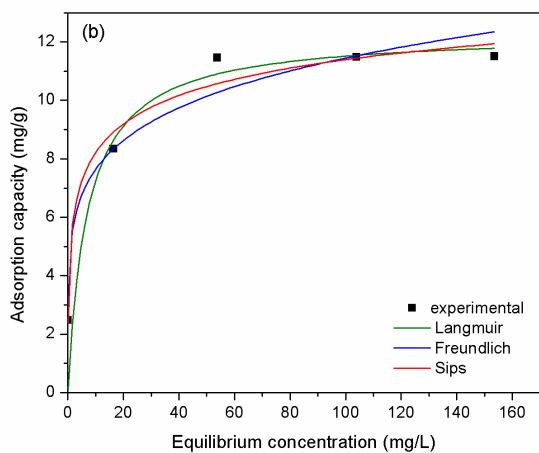
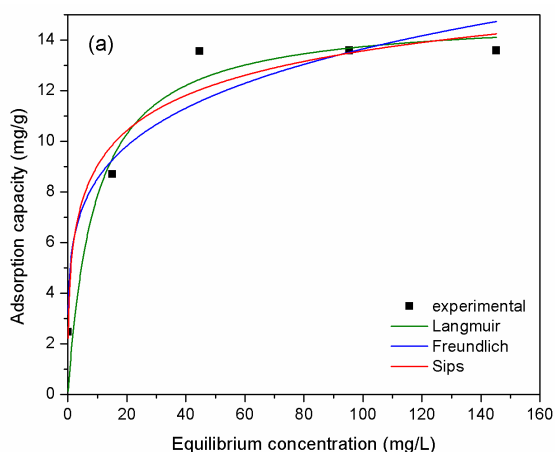


Fig. 8. Isotherm models for REEs adsorption onto magnesium silicate doped with Na- β -Gly-P (a) Eu(III), (b) Nd(III), (c) La(III).

Eu(III) adsorption onto magnesium silicate doped with Thi, Sips model has a R^2 value close to that of Langmuir isotherm, and the highest value of the heterogeneity factor $1/n_s$ (0.434), suggesting that in this case the adsorption mechanism is closest to the monolayer adsorption.

The maximum adsorption capacities of the REEs studied here reached using the thiourea doped magnesium silicate

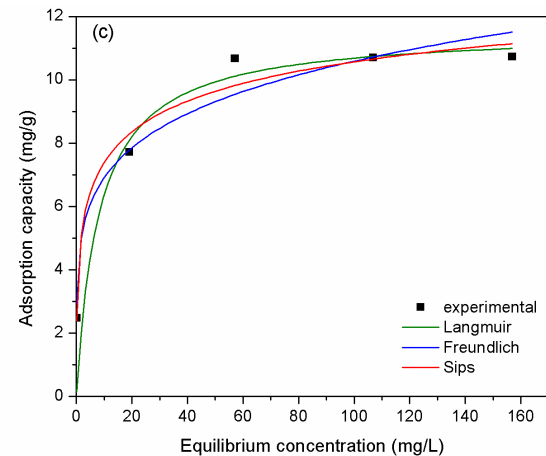
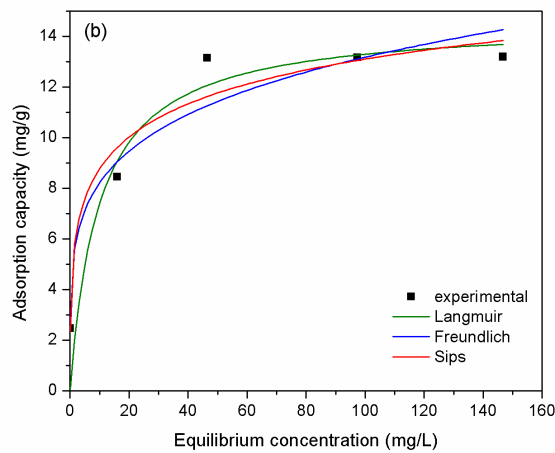
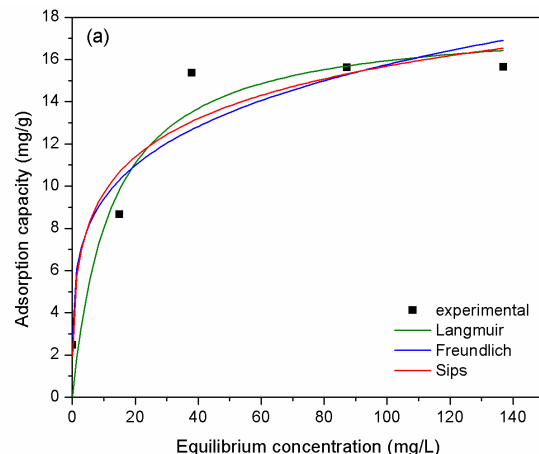


Fig. 9. Isotherm models for REEs adsorption onto magnesium silicate doped with TEABr (a) Eu(III), (b) Nd(III), (c) La(III).

were between 0.08 and 0.1 mol/kg. These values are close to other data reported in literature such as: 0.08 mol/kg for Nd(III) [38]. There were also reported higher capacities: 0.35 [39] and 1.18 mol/kg [40] for La(III), and 0.40 mol/kg for Nd(III) [39], but one should take into account that we obtained environmentally friendly adsorbents using a facile and non-pollutant method, and a very small extractant: support ratio.

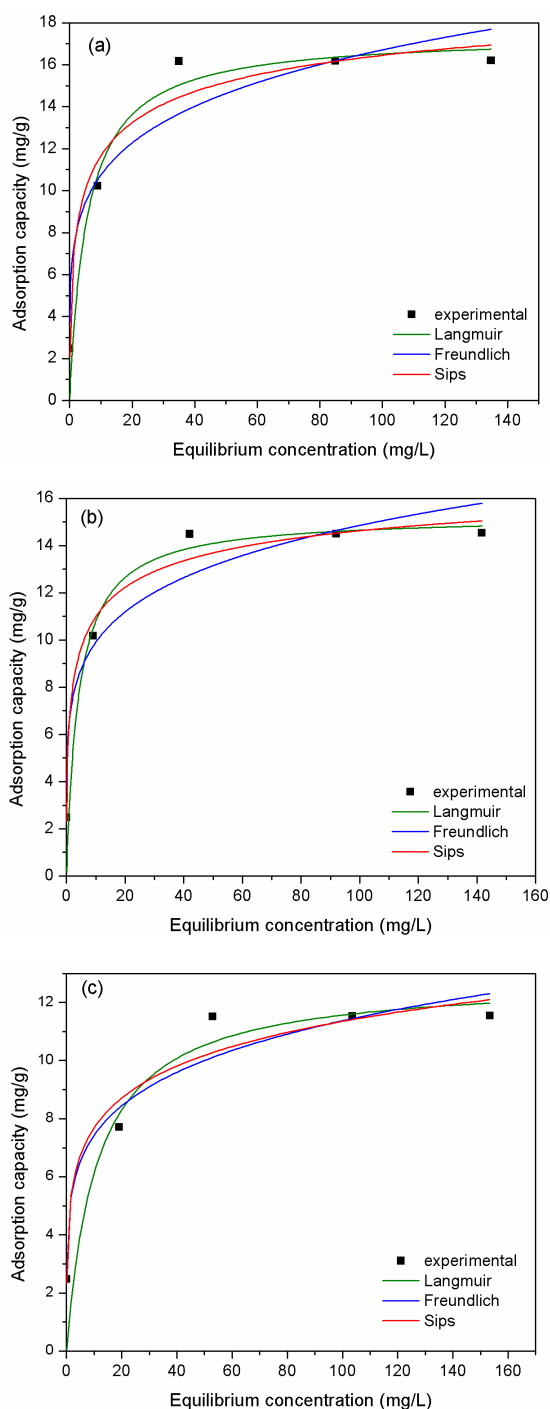


Fig. 10. Isotherm models for REEs adsorption onto magnesium silicate doped with Thi (a) Eu(III), (b) Nd(III), (c) La(III).

4. Conclusions

Magnesium silicate was doped with different environmentally friendly extractants (sodium β -glycerophosphate, tetraethylammonium bromide, and thiourea) through different methods: dry method, a method using ultrasounds, and the pellicular vacuum solvent vaporization. The doped materials were characterized by FTIR, SEM and EDX demonstrating the successful doping of the solid support. Of the three

doping methods, the pellicular vacuum solvent vaporization presented several advantages. Stirring time and drying time were significantly shorter, and the adsorption capacities of the materials obtained by this method were higher compared to the dry method and the method using ultrasounds. The obtained materials were used in order to remove some REEs (Eu(III), Nd(III), La(III)) from aqueous solutions. Best results were obtained when ethyl alcohol was used as solvent for the extractants, compared to using acetone, toluene, and n-hexane. The highest adsorption capacities were obtained for magnesium silicate doped with thiourea: 16.2 mg/g for Eu(III), 14.5 mg/g for Nd(III), and 11.5 mg/g for La(III). Our results show that these new obtained materials are efficient adsorbents and have potential applications in technologies for REEs recovery and for wastewater treatment.

References

- [1] S.U. Yesiller, A.E. Eroglu, T. Shahwan, Removal of aqueous rare earth elements (REEs) using nano-iron based materials, *J. Ind. Eng. Chem.*, 19 (2013) 898–907.
- [2] T.G. Goonan, Rare Earth Elements-End use and Recyclability: U.S. Geological Survey Scientific Investigations, Report 2011-5094, p. 15. Available online at: <http://pubs.usgs.gov/sir/2011/5094/>, 2011. (Accessed on 27 June, 2016).
- [3] İ. Çelik, D. Kara, C. Karadaş, A. Fisher, S.J. Hill, A novel ligand less-dispersive liquid-liquid microextraction method for matrix elimination and the preconcentration of rare earth elements from natural waters, *Talanta*, 134 (2015) 476–481.
- [4] P. Liang, Y. Liu, L. Guo, Determination of trace rare earth elements by inductively coupled plasma atomic emission spectrometry after preconcentration with multiwalled carbon nanotubes, *Spectrochim. Acta B*, 60 (2005) 125–129.
- [5] Y. Andrés, A.C. Texier, P. Le Cloirec, Rare earth elements removal by microbial biosorption: a review, *Environ. Technol.*, 24 (2003) 1367–1375.
- [6] M. Butnariu, P. Negrea, L. Lupa, M. Ciopec, A. Negrea, M. Pentea, I. Sarac, I. Samfira, Remediation of rare earth element pollutants by sorption process using organic natural sorbents, *Int. J. Environ. Res. Public Health*, 12 (2015) 11278–11287.
- [7] F. Ferrero, Adsorption of Methylene Blue on magnesium silicate: kinetics, equilibria and comparison with other adsorbents, *J. Environ. Sci.*, 22 (2010) 467–473.
- [8] F. Ciesielczyk, A. Krysztafkiewicz, T. Jesionowski, Magnesium silicates – adsorbents of organic compounds, *Appl. Surf. Sci.*, 253 (2007) 8435–8442.
- [9] L. Lupa, A. Negrea, M. Ciopec, P. Negrea, Cs⁺ removal from aqueous solutions through adsorption onto florasil impregnated with trihexyl(tetradecyl)phosphonium chloride, *Molecules*, 18 (2013) 12845–12856.
- [10] Z. Cai, J. Li., K. Liew, J. Hu, Effect of La₂O₃-doping on the Al₂O₃ supported cobalt catalyst for Fischer-Tropsch synthesis, *J. Mol. Catal. A Chem.*, 330 (2010) 10–17.
- [11] J.L. Cortina, A. Warshawsky, Developments in Solid-Liquid Extraction by Solvent-Impregnated Resins, Eds. J.A. Marinsky and Y. Marcus, Ion Exchange and Solvent Extraction, Marcel Dekker Publications; New York, NY, 1997, pp. 195–293.
- [12] M.M. Delgado-Povedano, M.D. Luque de Castro, A review on enzyme and ultrasound: A controversial but fruitful relationship, *Anal. Chim. Acta*, 889 (2015) 1–21.
- [13] K.S. Yoganand, M.J. Umaphathy, Green methodology for the recovery of Cr (IV) from tannery effluent using newly synthesized quaternary ammonium salt, *Arab. J. Chem.*, (2013). doi: 10.1016/j.arabjc.2013.02.022
- [14] Y. Akama, M. Ito, S. Tanaka, Selective separation of cadmium from cobalt, copper, iron(III) and zinc by water-based two-phase system of tetrabutylammonium bromide, *Talanta*, 53 (2000) 645–650.

- [15] Y. Akama, A. Sali, Extraction mechanism of Cr(VI) on the aqueous two-phase system of tetrabutylammonium bromide and $(\text{NH}_4)_2\text{SO}_4$ mixture, *Talanta*, 57 (2002) 681–686.
- [16] M. Noroozifar, M. Khorasani-Motlagh, Specific extraction of chromium as tetrabutylammonium-chromate and spectrophotometric determination by diphenylcarbazide: speciation of chromium in effluent streams, *Anal. Sci.*, 19 (2003) 705–708.
- [17] R. Niranjana, C. Koushik, S. Saravanan, A. Moorthi, M. Vairamani, N. Selvamurugan, A novel injectable temperature-sensitive zinc doped chitosan/ β -glycerophosphate hydrogel for bone tissue engineering, *Int. J. Biol. Macromol.*, 54 (2013) 24–29.
- [18] S. Kim, S.K. Nishimoto, J.D. Bumgardner, W.O. Haggard, M.W. Gaber, Y.A. Yang, chitosan/ β -glycerophosphate thermosensitive gel for the delivery of ellagic acid for the treatment of brain cancer, *Biomaterials*, 31 (2010) 4157–4166.
- [19] L. Wang, J.P. Stegemann, Thermogelling chitosan and collagen composite hydrogels initiated with β -glycerophosphate for bone tissue engineering, *Biomaterials*, 31 (2010) 3976–3985.
- [20] J. Chen, Y. He, C. Shan, Q. Pan, M. Li, D. Xia, Topical combined application of dexamethasone, vitamin C, and β -sodium glycerophosphate for healing the extraction socket in rabbits, *Int. J. Oral Max. Surg.*, 44 (2015) 1317–1323.
- [21] H.Y. Zhou, L.J. Jiang, P.P. Cao, J.B. Li, X.G. Chen, Glycerophosphate-based chitosan thermosensitive hydrogels and their biomedical applications, *Carbohydr. Polym.*, 117 (2015) 524–536.
- [22] J. Lisková, L. Bačaková, A.L. Skwarczyńska, O. Musiał, V. Bliznuk, K. De Schampelaere, Z. Modrzejewska, T.E.L. Douglas, Development of thermosensitive hydrogels of chitosan, sodium and magnesium glycerophosphate for bone regeneration applications, *J. Funct. Biomater.*, 6 (2015) 192–203.
- [23] R.C. Luckay, F. Mebrahtu, C. Esterhuysen, K.R. Koch, Extraction and transport of gold(III) using some acyl(aryl)thiourea ligands and a crystal structure of one of the complexes, *Inorg. Chem. Commun.*, 13 (2010) 468–470.
- [24] S. Facon, F. Adekola, G. Cote, Stripping of copper from CYANEX[®] 301 extract with thiourea-hydrazine-sodium hydroxide solution, *Hydrometallurgy*, 89 (2007) 297–304.
- [25] Y.S. Shelar, S.R. Kuchekar, S.H. Han, Extraction spectrophotometric determination of rhodium(III) with o-methylphenyl thiourea, *J. Saudi Chem. Soc.*, 19 (2015) 616–627.
- [26] A.E. Gabor, C.M. Davidescu, A. Negrea, M. Ciopec, M. Butnariu, C. Ianasi, C. Muntean, P. Negrea, Lanthanum separation from aqueous solutions using magnesium silicate functionalized with tetrabutylammonium dihydrogen phosphate, *J. Chem. Eng. Data*, 16 (2016) 535–542.
- [27] M. Ciopec, C.M. Davidescu, A. Negrea, L. Lupa, P. Negrea, A. Popa, C. Muntean, Use of D2EHPA-impregnated XAD7 resin for the removal of Cd(II) and Zn(II) from aqueous solutions, *Environ. Eng. Manage. J.*, 10 (2011) 1597–1608.
- [28] C.M. Davidescu, M. Ciopec, A. Negrea, A. Popa, L. Lupa, P. Negrea, C. Muntean, M. Motoc, Use of di-(2-ethylhexyl) Phosphoric Acid (DEHPA) impregnated XAD7 copolymer resin for the removal of chromium (III) from water, *Rev. Chim.*, (București), 62 (2011) 712–717.
- [29] P. Terzioğlu, S. Yücel, Synthesis of magnesium silicate from wheat husk ash: effects of parameters on structural and surface properties, *BioResources*, 7 (2012) 5435–5447.
- [30] V.Z. Vassileva, P.P. Petrova, Formation and characterization of bithiourea zinc formate, *Croat. Chem. Acta*, 78 (2005) 295–299.
- [31] E. Nor Hidawati, A.M. Mimi Sakinah, Treatment of Glycerin Pitch from biodiesel production, *Int. J. Chem. Environ. Eng.*, 2 (2011) 309–313.
- [32] J.D. Kubicki, K.W. Paul, L. Kabalan, Q. Zhu, M.K. Mroziak, M. Aryanpour, A.M. Pierre-Louis, D.R. Strongin, ATR-FTIR and density functional theory study of the structures, energetics, and vibrational spectra of phosphate adsorbed onto goethite, *Langmuir*, 28 (2012) 14573–14587.
- [33] K.S.W. Sing, Reporting physisorption data for gas/solid systems with special reference to the determination of surface area and porosity, *Pure Appl. Chem.*, 54 (1982) 2201–2218.
- [34] I. Langmuir, The adsorption of gases on plane surfaces of glass, mica and platinum, *J. Am. Chem. Soc.*, 40 (1918) 1361–1403.
- [35] H.M.F. Freundlich, Over the adsorption in solution, *J. Phys. Chem.*, 57 (1906) 385–470.
- [36] R. Sips, On the structure of a catalyst surface, *J. Phys. Chem.*, 16 (1948) 490–495.
- [37] A. Negrea, L. Lupa, M. Ciopec, C. Muntean, R. Lazau, M. Motoc, Arsenic removal from aqueous solutions using a binary mixed oxide, *Rev. Chim.*, (București), 61 (2010) 691–695.
- [38] A. Vlachou, B.D. Symeopoulos, A. Koutinas, A comparative study of neodymium sorption by yeast cells, *Radiochim. Acta*, 97 (2009) 437–441.
- [39] K. Dev, R. Pathak, G.N. Rao, Sorption behavior of lanthanum (III), neodymium (III), terbium (III), thorium (IV), and uranium (VI) on Amberlite XAD-4 resin functionalized with bicine ligands, *Talanta*, 48 (1999) 579–584.
- [40] S. Xu, Z. Wang, Y. Gao, S. Zhang, K. Wu, Adsorption of rare earths(III) using an efficient sodium alginate hydrogel cross-linked with Poly- γ -Glutamate, *PLoS ONE* (2015) 10(5): e0124826. doi: 10.1371/journal.pone.0124826